

# Coded Modulation for 100G Coherent EPON

Thomas Gerard, *Student Member, IEEE*, Hubert Dzieciol, *Student Member, IEEE*,  
Eric Sillekens, *Student Member, IEEE*, Yuta Wakayama, Alex Alvarado, *Senior Member, IEEE*,  
Robert I. Killey *Senior Member, IEEE*, Polina Bayvel, *Fellow, IEEE*, and Domanic Lavery, *Member, IEEE*

**Abstract**—Geometrically shaped (GS) 8-, 16, and 32-ary modulation formats are investigated for use in coherent passive optical networks. The modulation formats are designed to improve receiver sensitivity when paired with a binary, soft-decision forward error correction code (SD-FEC), such as a low density parity check (LDPC). Herein we consider the LDPC code specified in the draft 50G EPON standard, and show how this type of code can be particularly advantageous in a coherent transmission system. A receiver sensitivity of  $-26.7$  dBm is achieved at a post-FEC bit error rate below  $3.8 \times 10^{-6}$  for a polarization-scrambled 32-ary GS modulation format at 25 Gbd, received using a single-polarization, phase-diverse coherent receiver. This yielded a bit rate of 100 Gbit/s, net of coding and pilot overhead. This modulation format was shown to perform equally well in transmission, with no observed dispersion penalty after 80 km standard single mode fiber. Finally, this modulation format was received, at a reduced data rate of 50 Gbit/s, using a heterodyne coherent receiver based on a single balanced photodiode. The receiver sensitivity for this simplified receiver configuration was  $-28.5$  dBm, yielding a power budget of 34.2 dB.

**Index Terms**—Passive Optical Networks, Optical Fiber Communication, Advanced Modulation Formats, Digital Signal Processing

## I. INTRODUCTION

**I**NTENSITY modulation with direct detection (IM-DD), arguably the simplest optical fiber transmission scheme, has underpinned optical access networks since their inception. For transmission rates up to 10 Gbit/s/wavelength, this approach has worked well, and capitalizes on the relatively low cost of components for 10G-class communications.

However, for future systems operating at 25, 50, and 100 Gbit/s/wavelength, it seems likely that these ultra-low complexity systems will require support from digital signal

processing (DSP) for post-compensation of transmission impairments, such as chromatic dispersion. Further, in order to limit both the optoelectronic bandwidth requirements and dispersion penalty, possible upgrades to IM-DD systems include higher order modulation formats, which encode multiple bits per symbol, such as 4-ary pulse amplitude modulation (4PAM), and optical duobinary. Due to the combination of one-dimensional (i.e., amplitude) modulation and square law detection, the sensitivity penalty for migrating to multilevel IM-DD systems can be substantial [1].

For systems operating at 25 and 50 Gbit/s, the IEEE 802.3ca working group on Ethernet Passive Optical Networks (EPON) is considering the use of soft decision forward error correction (SD-FEC) based on low density parity check (LDPC) codes to improve the sensitivity margin of systems using on-off keying (OOK), thus extending the life of these low complexity systems [2].

In parallel to the developments in advanced IM-DD systems, the research community has also considered the use of low complexity coherent transmission systems, which use a local phase reference (i.e., a local oscillator or ‘LO’ laser) to enhance the receiver performance. The key advantages of coherent receivers in the context of a PON include:<sup>1</sup>

- an exceptionally high receiver sensitivity [5],
- frequency selectivity (i.e., optical filters are not inherently required in the receiver), and
- a linear detection profile.

The focus of this paper is the linear detection profile, as this enables the simultaneous use of both the optical amplitude and phase for modulation; i.e., two-dimensional modulation.

Conventional coherent systems use quadrature amplitude modulation (QAM), which is, for square QAM, the product of one-dimensional PAM modulation formats. However, QAM has previously been shown to be suboptimal for modulation in two-dimensions. By modifying the modulation format,  $M$ -ary signals can be optimized to improve receiver sensitivity; this process is called constellation shaping. However, the best modulation format to use depends upon the transmission channel, and whether the signal is coded or uncoded. If the system is coded, then one must also consider whether the signal is decoded using binary or nonbinary decoders, and whether the demapper makes a hard or soft decision on the received symbols.

In this work, we consider geometric shaping (GS), which changes the coordinates of the constellation to improve noise

Manuscript received April, 2019. This work was funded by United Kingdom (UK) Engineering and Physical Sciences Research Council (EPSRC) Programme Grant TRANSNET (Transforming networks - building an intelligent optical infrastructure), EP/R035342/1 T. Gerard and H. Dzieciol are in receipt of PhD studentships from the EPSRC and Microsoft Research. The work of A. Alvarado is supported by the Netherlands Organisation for Scientific Research (NWO) via the VIDI Grant ICONIC (project number 15685) and has received funding from the European Research Council (ERC) under the European Union’s Horizon 2020 research and innovation programme (grant agreement No 757791). D. Lavery is supported by the Royal Academy of Engineering under the Research Fellowships scheme.

T. Gerard, H. Dzieciol, E.Sillekens, R. I. Killey, P. Bayvel and D. Lavery are with the Optical Networks Group, Department of Electronic and Electrical Engineering, University College London, London WC1E 7JE, U.K. (e-mail: {thomas.gerard.15, hubert.dzieciol.18, e.sillekens, r.killey, p.bayvel, d.lavery}@ucl.ac.uk).

Y. Wakayama is with KDDI Corporation, 3-10-10 Iidabashi, Tokyo 102-8460, Japan. (e-mail: yu-wakayama@kddi.com).

A. Alvarado is with the Information and Communication Theory Lab, Signal Processing Systems Group, Department of Electrical Engineering, Eindhoven University of Technology, 5612 AZ Eindhoven, The Netherlands. (e-mail: a.alvarado@tue.nl).

<sup>1</sup>An excellent introduction to coherent receivers is available in [3], and a comprehensive discussion of the advantages of coherent receivers in PONs can be found in [4].

tolerance. While it is also possible to design improved constellations based on symbol probability (probabilistic shaping), such signals are less suitable for PON as they require computationally expensive demapping algorithms to achieve acceptable performance, which is not the case for two-dimensional GS.

In 2011, we experimentally investigated GS modulation formats for coherent PON [6], which were optimised for uncoded transmission systems (at asymptotically high signal-to-noise ratios) based on the earlier work of Karlsson and Agrell [7]. Crucially, these modulation formats were compared assuming the use of a hard decision FEC. As previously noted, there is a strong likelihood of future PONs incorporating soft decision FEC, and this changes the assumptions made in earlier work.

Therefore, in this paper, we revisit the topic of modulation format design for coherent PONs. Section II outlines the principle of geometric constellation shaping for two-dimensional modulation formats, and briefly describes the algorithm used for modulation format design. Section III describes the experimental configuration used to investigate the modulation formats, including a description of two low-complexity coherent receiver architectures. Section IV details the results of the investigation, and we conclude in Section V. Details of the modulation formats used in this work can be found in Section II and the Appendix.

## II. AN OVERVIEW OF GEOMETRIC SHAPING FOR POST-SD-FEC PERFORMANCE

### A. Geometrical Shaping

In optical communications system, there are several parameters, or dimensions, available for modulation. These include amplitude, phase, and optical frequency/wavelength. Further, each of these parameters can be modulated independently in each spatial mode of the transmission system. In a single mode optical fiber communication system, there are actually two modes available for transmission: the orthogonal X- and Y-polarizations.

In state-of-the-art optical access networks, only one dimension, amplitude, is used for modulation, and the wavelength domain is exploited for parallelism in the form of wavelength division multiplexing (WDM). In coherent systems, information about the phase of the optical carrier is also available, thus these systems can use two-dimensional modulation by simultaneously using both amplitude and phase.

Consider the constellation diagram shown in Fig. 1(e). This is the 16-ary quadrature amplitude modulation (16QAM) modulation format, which uses 16 phase and amplitude levels to encode 4 bits of information per symbol, as per the bit-to-symbol mapping shown<sup>2</sup>. This is a convenient modulation format to generate because the real- and imaginary-valued coordinates can be treated as the product of two independent 4PAM one-dimensional signals (generated  $\pi/2$  out of phase). The fact that the binary labeling is also a product labeling makes this constellation particularly attractive, because at the

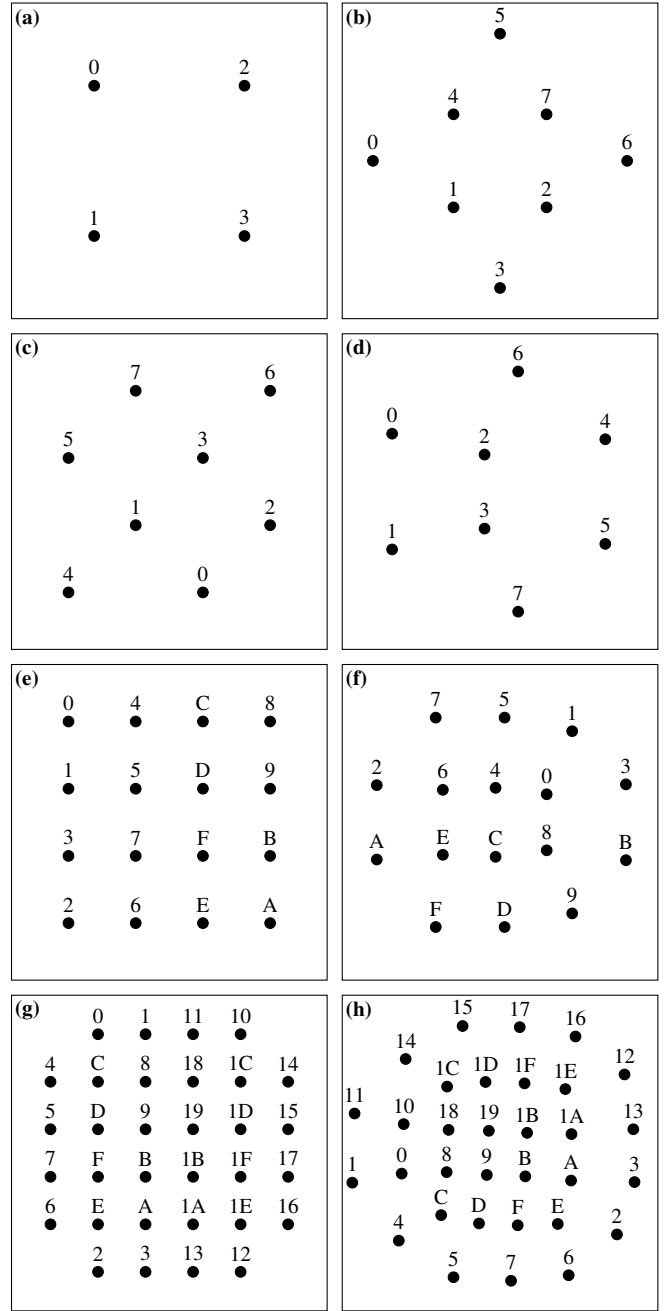


Fig. 1. The 2-dimensional modulation formats used in this work; for the purpose of this paper, the horizontal and vertical dimensions can be treated as the real and imaginary axes, respectively. The bit-to-symbol mappings used (i.e., the binary labeling) are shown in hexadecimal for brevity, but are given alongside the constellation coordinates in the Appendix. The constellation diagrams show (a) QPSK, (b) Star 8QAM, (c) DSQ<sub>28</sub>, (d) GS<sub>28</sub> (a 2-dimensional 8-ary modulation format optimized for performance at a GMI of 2.625 bit/symbol), (e) 16QAM, (f) GS<sub>216</sub> (optimized at 3.5 bit/symbol), (g) 32QAM, and (h) GS<sub>232</sub> (optimized at 4.375 bit/symbol).

receiver the detection can be performed per-dimension, independently. The relative simplicity of generation and encoding is the reason for its prevalence in both research and commercial communication systems. However, for an additive white Gaussian noise (AWGN) channel, 16QAM is not necessarily the optimal choice of modulation format. In fact, the optimum choice of modulation format depends on the signal-to-noise

<sup>2</sup>For all constellations discussed in this work, the exact coordinates and mappings are given in the Appendix.

ratio (SNR) and, additionally, on whether hard-decision or soft-decision FEC is used for encoding and decoding the signal [8], [9], [16].

**B. Performance Metrics**

The LDPC code used in the draft EPON standard has a block length of 17664 to carry 14592 information bits<sup>3</sup>. To design the communication system optimally, the modulation format needs to be chosen to match this particular code. However, designing modulation formats with respect to a specific SD-FEC code is non-trivial. Furthermore, it is not desirable to have to redesign the modulation format each time the FEC is changed.

Fortunately, information-theoretic metrics exist which allow the designer to abstract the format design from the specific FEC, but still consider different types of FEC [8], [9]. Here we summarise the three most popular metrics that can be used for geometrically-shaped formats:

- **Mutual information:** Used to find the minimum SNR of an ideal *nonbinary* soft-decision FEC encoder-decoder pair [10],
- **Generalised mutual information (GMI):** Used to find the minimum SNR of an ideal *binary* soft-decision FEC encoder-decoder pair [11], [12], and
- **Pre-FEC BER (SER):** Used to find the minimum SNR of an ideal binary (nonbinary) hard decision FEC code [9].

As this work focuses on binary SD-FEC performance, the modulation formats are optimized with respect to GMI.

Under the assumption of an AWGN channel—a reasonable assumption for a coherent PON—GMI can be calculated via numerical integration using Gauss-Hermite quadratures, which is the approach taken here. This method computes the contribution of each bit position to the information content of the transmitted signal; i.e., for 16QAM, it is the summation of the information conveyed by each of the four possible bits encoded by a 16QAM symbol. A detailed description of how to compute GMI is provided in [8], [12], so will not be reiterated here.

**C. Optimizing Modulation Formats for EPONs**

All the constellations used in this work are shown in Fig. 1. Standard square QAM formats are shown in Fig. 1(a), (e), and (g), with a Gray bit-to-symbol mapping. The optimized constellations are shown in Fig. 1(d), (f) and (h), and are herein known as GS2<sub>8,16,32</sub> for 8-, 16-, and 32-ary modulation, respectively.

To design the GS modulation formats for the EPON LDPC code, we optimized the constellations to minimize the SNR penalty at the *GMI threshold* of the LDPC decoder. The GMI threshold—the maximum value of GMI required to successfully decode any given codeword from the LDPC decoder—is estimated in section IV. We determine this value to be a GMI of 0.875*m* bit/symbol where *m* is the (gross) number of bits transmitted per symbol. Therefore, the constellations

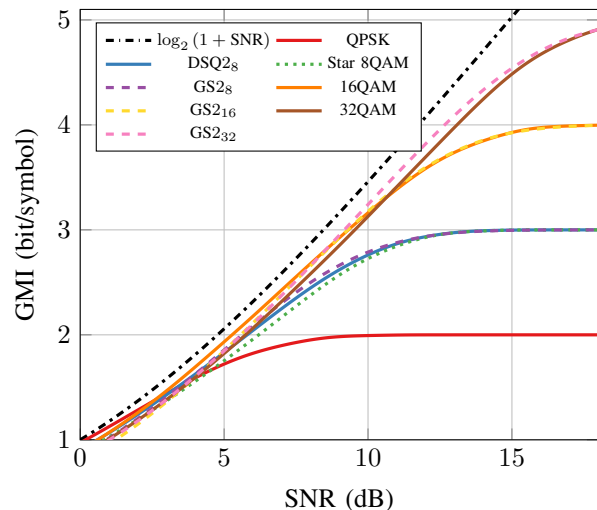


Fig. 2. The theoretical GMI performance of all eight modulation formats considered in this work.

were optimized to minimize the SNR requirements for a GMI of 0.875*m* bit/symbol.

The methodology used for optimization is based on gradient descent (as per the first design stage in [13]) but with optimization of the bit-to-symbol mapping during the gradient descent using the binary label switching algorithm as per [14], [15]. This process is not guaranteed to find the globally optimum constellation, but the resulting constellations demonstrably improve performance versus the conventional modulation formats. The resulting 16-ary constellation is as per the optimized curve shown in [16], but at an optimized SNR of approximately 11.3 dB. 8- and 32-ary constellations are not discussed in [16], but the overall optimization procedure is similar.

Finally, we also include two well-known shaped 8-ary formats for comparison. Star 8QAM, Fig. 1(b), which is often used for optical communications systems [17]–[19], and DSQ<sub>28</sub>; another 2-dimensional, 8-ary modulation format which has found application in, for example, cable communications networks [20].

The performance of these modulation formats can be determined by numerical estimation of the GMI for a given SNR, and the result of this comparison is shown in Fig. 2. For a coherent transmission system corrupted only with AWGN gains in SNR translate into gains in power sensitivity [21]. For a code rate of 0.826, as per the EPON FEC, the upper bound on achievable information rate is 0.826*m*. Practical FEC codes operate at a penalty with respect to capacity and so, for the code considered herein, the required GMI is actually 0.875*m*, as previously noted. At a GMI of 0.875*m*, Fig. 2, shows that QPSK signalling requires an SNR of 5.2 dB. This increases to 9.3, 9.0, and 8.8 dB for Star 8QAM, DSQ<sub>28</sub> and GS<sub>28</sub>, respectively. Therefore, the theoretical gain in SNR margin for GS<sub>28</sub> is 0.5 dB versus Star 8QAM at this GMI.

For 16QAM and GS<sub>16</sub> the SNR requirements are 11.55 and 11.47 dB, respectively. Because of the relatively good performance of square QAM at high code rates, there is

<sup>3</sup>A code rate of 0.826 before shortening and puncturing.

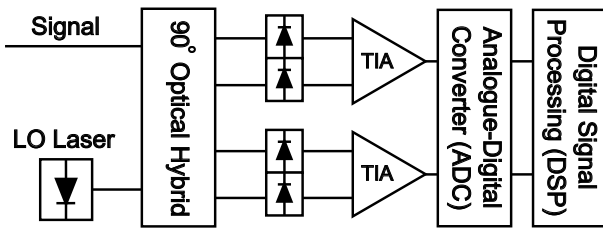


Fig. 3. A simplified, phase-diverse, coherent receiver based on a  $90^\circ$  optical hybrid and two balanced photodetectors (for in-phase and quadrature detection).

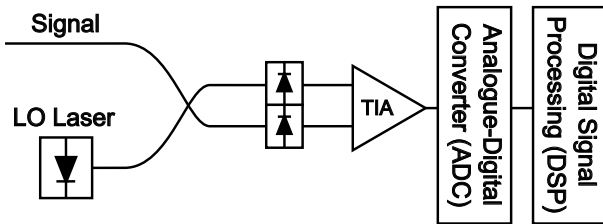


Fig. 4. A simplified coherent receiver based on a single balanced photodetector and heterodyne detection.

theoretically very little to gain (0.07 dB in SNR) for geometric shaping.

Finally, for 32QAM and GS<sub>232</sub> the SNR requirements are 14.5 and 14.2 dB, respectively, indicating that 0.3 dB in SNR margin can be gained by geometric shaping. As previously noted, the SNR gain for all these formats depends on the SNR and the specific type of FEC code assumed in the constellation optimization. Note also that similar gains in SNR have been observed for shaped 32-ary modulation formats as discussed in [22] (and references therein) when applied to long-haul transmission systems.

Note that the LDPC FEC code itself has been robustly verified, and exhibits no error floor at post-FEC BERs below  $10^{-12}$  [23].

### III. EXPERIMENTAL CONFIGURATION

#### A. Transceiver Design

In long-haul optical fiber communication systems, it is conventional to use a coherent receiver which is both phase- and polarization-diverse. This allows parallel transmission of data in both polarization modes. For reasons discussed in [24], it is desirable to minimise the optical complexity of the receivers used in the ONU, which can be achieved by sacrificing polarization diversity. In this paper, we present two architectures which achieve this simplification.

Fig. 3 shows a coherent receiver which is suitable for intradyne detection (i.e., the wavelength of the LO laser is comparable to the wavelength of the signal). The use of a  $90^\circ$  optical hybrid allows both the real- and imaginary-valued spectral components to be recovered [3]. A further simplification, shown in Fig. 4, removes the optical hybrid and one balanced photodetector (BPD). Thus in this receiver the signal is recovered with a single BPD, but the receiver operation is then restricted heterodyne coherent detection (i.e., the LO laser wavelength must be offset from the signal by

more than half the symbol rate, such that the received signal can be assumed to be real-valued). There is an inherent 3 dB sensitivity penalty for this approach due to shot noise aliasing, and this is discussed in [4].

In both cases, the receiver is polarization-selective. That is, the receivers will only detect signals which are incident on the photodetectors with the same state of polarization as the LO laser. Several options are available to circumvent this limitation [4], but herein we consider OLT-side polarization scrambling. In this technique, discussed in detail in [4], [25], and first proposed in [26], a single-polarization data signal generated by the transmitter at a symbol rate,  $F_s$ , is forced into an orthogonal polarization state at a rate  $2F_s$ , such that it is guaranteed that the signal will beat with the LO laser 50% of the time.

#### B. PON Configuration

The experimental configuration used to emulate the PON is shown in Fig. 5. An external cavity laser (ECL)<sup>4</sup> with linewidth  $\sim 100$  kHz emitting at 1550 nm was coupled into a dual-polarization IQ Mach Zehnder modulator (IQ MZM). This was driven by a 92 GS/s, 8 bit digital-to-analogue converter (DAC) with a 3 dB bandwidth of 32 GHz for data generation. After modulation, the signal was amplified using an erbium-doped fiber amplifier (EDFA) with a noise figure of 5 dB, before being attenuated to 6 dBm launch power. The signal was transmitted over 80 km of standard single-mode fiber (SSMF) with 16 dB of loss and a dispersion parameter of 16 ps/(nm.km). After transmission, splitting-loss was emulated using a variable optical attenuator (VOA), which was also used to vary the optical power incident on the receiver. This was monitored using a 3 dB tap and optical power meter. The simplified, phase-diverse coherent receiver shown in Fig. 3 was emulated by using a dual-polarization coherent receiver where only the X-polarization photodiodes were powered. A  $90^\circ$  optical hybrid was used to mix the received signal with a local oscillator (LO), permitting recovery of both in-phase and quadrature components. The LO was a second ECL, whose output was passed directly to the  $90^\circ$  optical hybrid. The LO power was set to be 7.8 dBm per BPD in all cases. The frequency offset between the signal and LO was set to be below 200 MHz. The X-polarization beat signal was detected using two BPDs then digitised using a 50 GS/s digital sampling oscilloscope with a 3 dB bandwidth of 22 GHz.

To emulate the heterodyne coherent receiver shown in Fig. 4, the physical setup described above was unchanged. However, only one the signal incident on one of the BPDs was captured and processed. Due to the bandwidth limitation of the digital sampling oscilloscope, the symbol rate was necessarily halved to 12.5 GBd. The LO laser frequency was increased by 14 GHz satisfy the minimum phase condition required for phase-diverse recovery from a real signal [28].

<sup>4</sup>The use of an ECL was intended to be indicative of the performance of modern, integrable, widely-tunable, C-band lasers. One such example is the Digital Supermode Distributed Bragg Reflector (DSDBR) laser, which exhibits similar characteristics to the ECLs used herein, while being suitable for volume manufacturing [27].

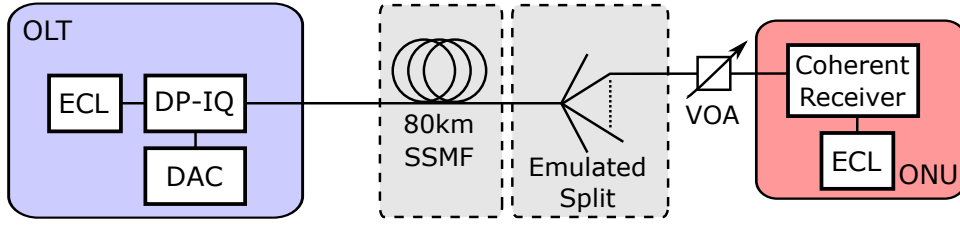


Fig. 5. The experimental configuration used to evaluate the performance of the simplified coherent receivers using advanced modulation formats. The splitter loss is emulated by the VOA: variable optical attenuator. The DAC produces a precoded signal which simultaneously modulates the data and applies the polarization scrambling using the DP-IQ modulator in the OLT.

C. Digital Signal Processing

We generated 25 EPON codewords, each of 17664 bits (14592 information bits). The codewords were sequentially mapped to data frames of  $2^{16}$  symbols. The number of codewords per data frame is described by

$$N_{CW} = \left\lfloor \frac{(N_S - N_{\text{pilot}}) \times m}{n_{CW}} \right\rfloor,$$

where  $N_S$  is the number of symbols per data frame,  $N_{\text{pilot}}$  is the number of pilot symbols per data frame (discussed in the following paragraph) and  $n_{CW}$  is the number of bits per codeword. Therefore, the number of measurable information bits, and hence the minimum measurable BER,  $\text{BER}_{\text{min}}$ , is dependent on  $m$ . Table I summarises this information. The error-free results reported in this paper are, therefore, at least lower than the  $\text{BER}_{\text{min}}$  associated with the modulation format under test.

TABLE I  
NUMBER OF CODEWORDS USED DEPENDING ON MODULATION FORMAT

$m$	$N_{CW}$	$\text{BER}_{\text{min}}$
2	7	$9.8 \times 10^{-6}$
3	10	$6.9 \times 10^{-6}$
4	14	$4.9 \times 10^{-6}$
5	18	$3.8 \times 10^{-6}$

Eight modulation formats were tested: QPSK, Star 8QAM, DSQ2<sub>8</sub>, GS2<sub>8</sub>, 16QAM, GS2<sub>16</sub>, 32QAM and GS2<sub>32</sub>. From Fig. 1, we can see that the outer constellation points of the GS modulation formats are more compressed than their square counterparts; we found this made accurate frequency-offset estimation and carrier phase recovery challenging. To correct for this, QPSK pilot symbols were inserted between the transmitted symbols. 1024 pilot symbols were used at the start of the symbol sequence, then a pilot symbol was inserted every 64<sup>th</sup> symbol position thereafter. This amounted to a transmission overhead of 3.1%. This pilot DSP technique, which is further detailed in [29], [30], was used for all formats except QPSK. Although geometrically shaped modulation formats can be demodulated without pilot symbols, the use of pilot symbols decouples the impact of the DSP algorithm design from the modulation format, and allows for repeatable measurements [29]. Once mapped, the symbol-sequence was polarization scrambled. The signal was Nyquist-shaped with a roll-off factor of 0.1, then uploaded to the DAC such that

signals were generated at 25 GBd, with a 50 GHz polarization scrambling rate.

After detection, the digitised signal was normalised and the effects of chromatic dispersion were corrected for using a 15 tap FFT equalizer [31]. The location of the pilot symbols were determined using the minimum-error terms of an 11 tap equalizer based on the constant modulus algorithm (CMA); these symbols were then used to measure and correct for frequency offset between the signal and LO lasers. The 1024 pilot header symbols were isolated and passed through an 11 tap T/2-spaced CMA equalizer to estimate the required weights for the payload; we then used these output tap weights to initialise the 11 tap CMA equalizer applied to the payload symbols. Viterbi-Viterbi carrier phase estimation (21 taps) was performed using the pilot symbols inserted within the payload symbols; the resulting phase estimates were interpolated and applied to the entire payload. Finally, a 21 tap maximum likelihood phase estimator was applied to the payload. Empirically we found that 31 taps offered the best performance in the transmission experiments.

The heterodyne receiver was processed in the same way as described above, however with the additional step of digitally down-converting the one-sided information spectrum to base-band to correct for the LO offset. We observed that, without phase-diversity, the frequency offset estimation accuracy was impaired. Therefore the Viterbi-Viterbi phase estimation was decreased to 7 taps to enable fast tracking of any residual frequency offset.

It is worth noting that the above DSP chain is essentially unchanged versus a conventional dual-polarization coherent receiver. Despite the polarization scrambling, a T/2-spaced adaptive equalizer was still sufficient for signal recovery.

After equalization, the payload symbols were extracted and demapped to recover all the transmitted codewords. We passed each codeword through the LDPC decoder individually to test their real performance. The LDPC decoder was the 0.826-rate code implemented with 15 iterations, as per the draft EPON standard. Here we report the average bit error rate (BER) both before and after correction by performing a bit-wise comparison of the transmitted and recovered codewords. Reported data rates are specified as either line rate (excluding overhead) or data rate (including FEC and pilot overheads).

IV. RESULTS AND DISCUSSION

A. Back-to-back Verification of GS Modulation Formats

For each modulation format, the received signal power onto the simplified coherent receiver was varied in steps of 0.25 dB around the FEC threshold and in steps of 1 dB at higher powers. At each point, the received signal power was measured using the optical power meter to a precision of  $\pm 0.005$  dB. The signal was then captured and BER pre- and post-FEC were measured. These results are shown in Fig. 6. Magnifications of the 8-ary and 32-ary plots are shown at a BER of  $2.7 \times 10^{-2}$  are shown to appreciate the gains around the FEC limit. Of the 8-ary formats, the GS<sub>8</sub> is measured to outperform the Star 8QAM by 0.75 dB, and the DSQ<sub>8</sub> by 0.2 dB. This is slightly greater than the estimated theoretical shaping gain of 0.5 dB, which we attribute to impaired DSP performance for Star 8QAM. The 0.2 dB gain over DSQ<sub>8</sub> is in line with theoretical predictions. The GS<sub>8</sub> signal was measured as error free after FEC at  $-32.7$  dBm.

For 16-ary modulation, GS<sub>16</sub> was measured to outperform 16QAM by less than 0.1 dB, also in line with theory. The GS<sub>32</sub> outperforms 32QAM by 0.25 dB; again, in good agreement with the theoretical gain of 0.3 dB. The GS<sub>32</sub> was measured to be error free at  $-26.7$  dBm while sustaining a data rate of 100 Gb/s (line rate 125 Gb/s). The received powers at which each format was measured to be error free are summarised in Table II.

B. Experimental Evaluation of EPON LDPC Code Performance

As outlined in section II(c), the geometrically shaped constellations have been optimised for a GMI of  $0.875m$ . At this

TABLE II  
BACK TO BACK RECEIVED POWERS REQUIRED FOR POST-FEC ERROR FREE PERFORMANCE AND RESULTANT DATA RATE

Format	Received Power (dBm)	Data Rate (Gb/s)
QPSK	-36.79	41.31
Star 8QAM	-31.94	60.04
DSQ <sub>8</sub>	-32.47	60.04
GS <sub>8</sub>	-32.69	60.04
16QAM	-29.69	80.06
GS <sub>16</sub>	-29.49	80.06
32QAM	-26.43	100.07
GS <sub>32</sub>	-26.73	100.07

GMI, all transmitted data should be recoverable after FEC. To experimentally measure this, the normalised GMI ( $GMI/m$ ) was calculated for all the post-FEC data points presented in Fig. 6 by taking  $GMI/m$ . This data is presented in Fig. 7. We can see that all the different modulation formats perform similarly when considered in terms of  $GMI/m$ . The inset of Fig. 7 shows that for  $GMI/m$  higher than 0.875 all data is error-free. By taking an average of the  $GMI/m$  immediately before and after each format becomes error free, the  $GMI/m$  threshold is experimentally measured as  $0.875 \pm 0.004$ .

C. 80 km Transmission of GS<sub>32</sub> Signal

Finally, to demonstrate that the linear coherent receiver profile is preserved, even with polarization scrambling, a GS<sub>32</sub> signal was transmitted over 80 km of fiber using two receiver setups: the simplified coherent receiver and the single BPD detection. For each configuration, we measured the received signal power, BER pre- and post-FEC as shown in

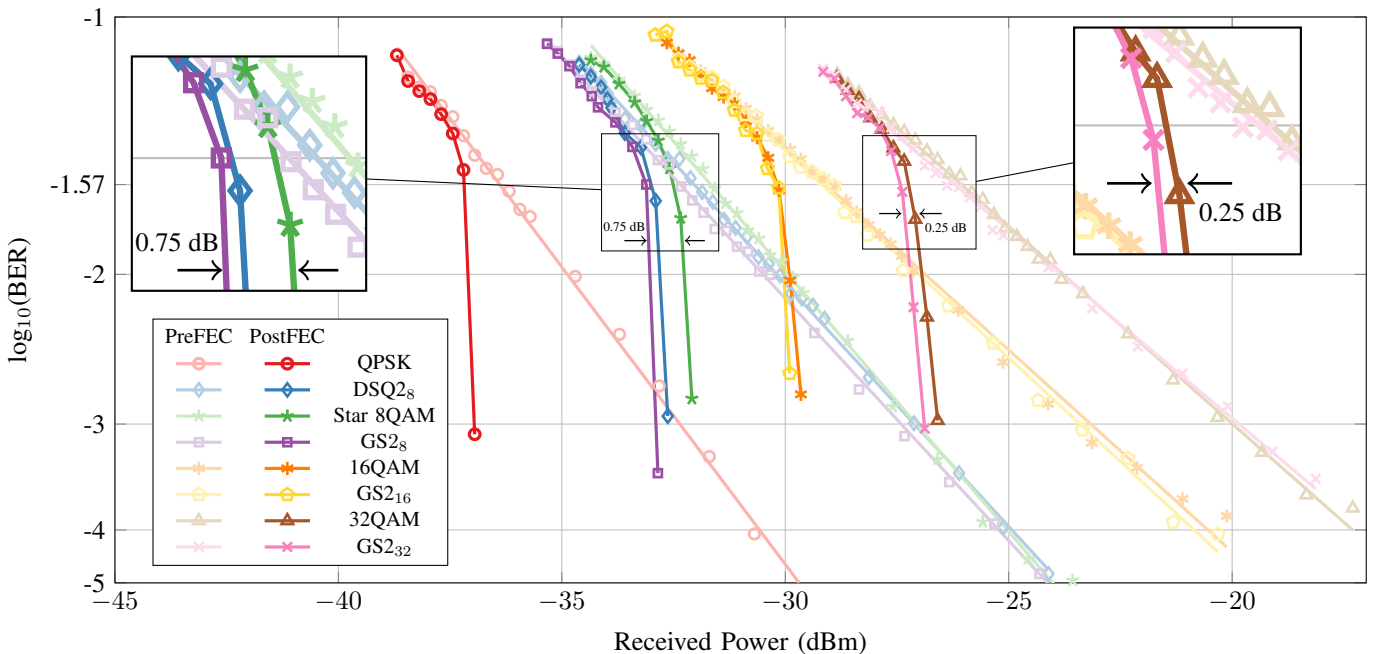


Fig. 6. Back-to-back performance of 25 Gb/s, polarization scrambled formats, with and without geometric shaping, received using the simplified coherent receiver. Both pre- and post-FEC results are presented.

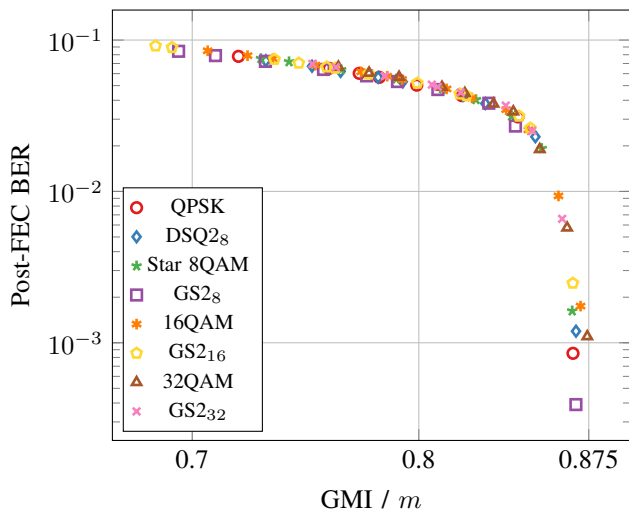


Fig. 7. Normalised generalised mutual information ( $GMI / m$ ) for all the data presented in Fig. 6 plotted against post-FEC BER. All data above a ( $GMI / m$ ) of 0.875 is error free.

Fig. 8. Using the simplified coherent detection at 25 GBd, we demonstrated post-FEC error-free performance at  $-26.7$  dB. Compared with back-to-back results, the 80 km transmission shows no performance penalty due to chromatic dispersion of the fiber. Therefore, we claim a loss budget of 32.7 dB based on the launch power of 6 dBm.

The 80 km transmission using a single BPD demonstrated post-FEC error-free performance at  $-28.5$  dBm. Due to the receiver bandwidth limitation, the symbol rate of this configuration was reduced to 12.5 GBd, yielding a net data rate of 50 Gbit/s. The loss budget for this system is, therefore, 34.5 dB. As noted previously, the single BPD receiver suffered from frequency offset estimation issues after transmission. This introduced an error floor, which can be clearly seen in the pre-FEC results of Fig. 8. Nevertheless, the signal had sufficient SNR margin to be completely recovered after the LDPC decoder<sup>5</sup>.

The issues with the heterodyne coherent, single BPD receiver highlight an important design trade-off. Although the receiver can be easily implemented with an optical front end consisting of a 2x2 coupler and an LO laser, the bandwidth requirements are double (and in practice, more than double) that of the equivalent intradyne receiver. However, the removal of the optical hybrid decreases the insertion loss of the receiver, which in turn, improves the receiver sensitivity. Some of the bandwidth requirements can be mitigated by using higher order modulation formats, but such an investigation is outside the scope of this paper.

Finally, we emphasise that for both receiver architectures considered herein, optical filters were not used, and were not required in the receiver. Receiver architectures based on tuneable optical filtering in the ONU (e.g., NG-PON2) will exhibit an excess insertion loss due to filtering. When

comparing the above results with such systems, this additional penalty for IM-DD systems should always be considered.

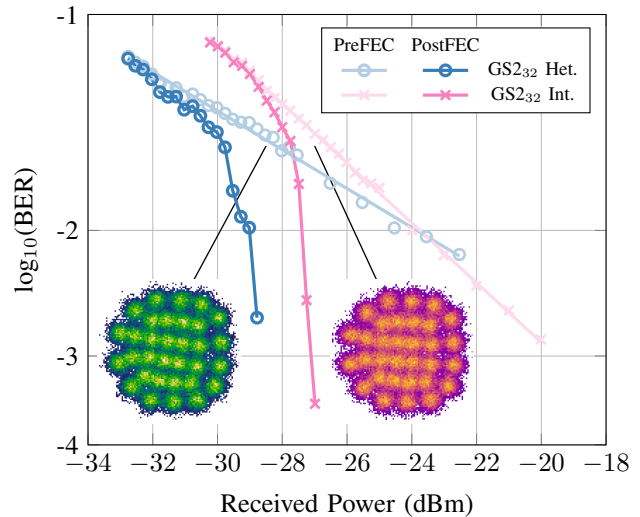


Fig. 8. 80 km transmission of polarization scrambled  $GS_{232}$  using a simplified intradyne coherent receiver (*Int.*) and a single balanced photodiode (BPD) heterodyne coherent receiver (*Het.*) at 25 GBd and 12.5 GBd respectively. The inset constellation diagrams recover post-FEC error free.

## V. CONCLUSION

The performance of a simplified coherent receiver, with the potential for use in an ONU, was demonstrated with power- and bandwidth-efficient advanced modulation formats. By varying the order of modulation between 4- and 32-ary QAM, it was shown that the information rate per channel can be scaled to over 100 Gbit/s per channel, albeit with a sensitivity penalty incurred by the increased order of modulation.

Geometrically shaped modulation formats were therefore designed to enhance the sensitivity of the transmission system assuming the use of a rate 0.826 LDPC FEC code specified by the IEEE 802.3ca draft 25/50G EPON standard. The optimised modulation formats provided sensitivity gains up to 0.75 dB after LDPC decoding versus conventional QAM formats, showing that, even for coherent systems, coded modulation with LDPC decoders can have non-trivial implications for receiver sensitivity.

The simplified coherent receiver design, based on a polarization-scrambling OLT and a dual BPD ONU was demonstrated using a 25 GBd 32-ary geometrically shaped channel, which was transmitted over 80 km SSMF. Due to the linearity of the coherent receiver, this transmission scheme incurred no dispersion penalty, and achieved a sensitivity of  $-26.7$  dBm. With an EPON-compatible launch power of 6 dBm, this lead to a power budget of 32.7 dB; exceeding the PR30 EPON standard requirement whilst achieving a net data rate of over 100 Gbit/s.

A further simplification to the ONU was investigated by implementing a heterodyne coherent receiver with only a single BPD and a reduced, 12.5 GBd, symbol rate. This configuration achieved a  $-28.5$  dBm sensitivity, leading to a 34.5 dB power budget at a net data rate of over 50 Gbit/s.

<sup>5</sup>Note that in Fig. 8, although the actual receiver configuration was unchanged, the receiver loss has been calibrated to show the equivalent loss of a receiver incorporating a 2x2 coupler (assumed loss 3.5 dB).

This exceeds both the PR30 and PR40 standard requirements. The symbol rate was limited in this latter investigation due to the increased optoelectronic bandwidth requirements of this heterodyne configuration.

It should be noted the theoretical performance of the single BPD (heterodyne) receiver at 12.5 GBd and the dual BPD (intradyn) receiver at 25 GBd is equivalent, for the reasons noted in Section III-A. However, because the heterodyne receiver does not require an optical hybrid, the insertion loss of the receiver was reduced, thus improving the receiver sensitivity. Therefore, if the intradyne receiver were to be operated at 12.5 GBd, the receiver sensitivity would outperform the 12.5 GBd heterodyne receiver by only 1.2 dB, albeit with a reduced optoelectronic bandwidth requirement.

Taken together, these two results can be viewed as one potential road map for increasing the data rates of EPON beyond 50 Gbit/s/wavelength, but without the substantial optoelectronic requirements of phase- and polarization-diverse coherent receivers.

APPENDIX  
COORDINATES AND BINARY LABELINGS FOR  
GEOMETRICALLY SHAPED MODULATION FORMATS

The modulation formats used herein can be broadly divided into ‘standard’ QAM and geometrically shaped constellations. 4-, 16- and 32-ary QAM are well-known modulation formats, with well-defined Gray binary labelings, and will therefore not be detailed here.

Two of the 8-ary constellations are also well-defined in the literature. Star 8QAM and DSQ<sub>28</sub> are both discussed in [17], and coordinates and asymptotic performance metrics for these formats are available via an online database of codes and constellations, curated by Prof. Erik Agrell [32].

The remaining formats are the GS 8-, 16-, and 32-ary constellations. Table III lists the coordinates of the constellation points and the bit-to-symbol mapping assumed in this work. The constellations are assumed to be normalised to unit power; that is, with a root mean square value of 1.

ACKNOWLEDGMENT

The authors wish to extend their thanks to Dr Jun Shan Wey for enlightening discussions, particularly on the topic of the IEEE 802.3ca LDPC code. We are grateful to Dr Lidia Galdino for technical support throughout the experiment, and Dr Sezer Erkilinc for discussions on simplified coherent receivers. Finally, we wish to thank Oclaro Inc. for the high speed, dual polarization, IQ modulators used in this work.

REFERENCES

[1] V. Houtsma and D. van Veen, “Bi-Directional 25G/50G TDM-PON With Extended Power Budget Using 25G APD and Coherent Detection,” *J. Lightwave Technol.* vol. 36, no. 1, pp. 122-127, 2018.  
 [2] IEEE P802.3ca 50G-EPON Task Force [Online]. Available: <http://www.ieee802.org/3/ca/>.  
 [3] K. Kikuchi, “Fundamentals of Coherent Optical Fiber Communications,” *J. Lightwave Technol.*, vol. 34, no. 1, pp. 157-179, Jan., 2016.  
 [4] M. S. Erkilinc, D. Lavery, K. Shi, B. C. Thomsen, R. I. Killey, S. J. Savory, and P. Bayvel, “Comparison of Low Complexity Coherent Receivers for UDWDM-PONs ( $\lambda$ -to-the-User),” *J. Lightwave Technol.* vol. 36, no. 16, pp. 3453-3464, Aug., 2018.

TABLE III  
BINARY LABELING AND COORDINATES OF CONSTELLATION POINTS FOR GS MODULATION FORMATS (TO 4 DECIMAL PLACES)

Binary	Constellation		
	GS <sub>28</sub>	GS <sub>16</sub>	GS <sub>32</sub>
00000	(-1.4362,0.7701)	(-0.6517,0.3917)	(-1.3091,-0.2737)
00001	(-1.4362,-0.7701)	(-1.0078,1.2731)	(-1.9660,-0.3945)
00010	(-0.2060,0.4925)	(1.7226,0.5190)	(1.5558,-1.0831)
00011	(-0.2060,-0.4925)	(-1.7590,0.5304)	(1.7896,-0.3862)
00100	(1.4008,0.6961)	(0.06231,0.4819)	(-1.3474,-1.1657)
00101	(1.4008,-0.6962)	(-0.06329,1.4631)	(-0.6190,-1.6528)
00110	(0.2414,1.5981)	(0.7992,0.4538)	(0.9132,-1.6261)
00111	(0.2414,-1.5981)	(0.8989,1.4627)	(0.1467,-1.6996)
01000	-	(-0.6519,-0.3914)	(-0.7106,-0.2543)
01001	-	(-1.0084,-1.2727)	(-0.1762,-0.2915)
01010	-	(1.7224,-0.5197)	(0.9454,-0.3661)
01011	-	(-1.7592,-0.5297)	(0.3365,-0.3107)
01100	-	(0.0621,-0.4819)	(-0.7832,-0.8264)
01101	-	(-0.06388,-1.4632)	(-0.2800,-0.9371)
01110	-	(0.7990,-0.4542)	(0.7683,-0.9438)
01111	-	(0.8983,-1.4630)	(0.2351,-0.9612)
10000	-	-	(-1.2817,0.3846)
10001	-	-	(-1.9357,0.5261)
10010	-	-	(1.6566,1.0459)
10011	-	-	(1.7736,0.3166)
10100	-	-	(-1.2557,1.2513)
10101	-	-	(-0.4983,1.6902)
10110	-	-	(1.0042,1.5507)
10111	-	-	(0.2624,1.6752)
11000	-	-	(-0.6847,0.3082)
11001	-	-	(-0.1490,0.2958)
11010	-	-	(0.9507,0.2519)
11011	-	-	(0.3604,0.2687)
11100	-	-	(-0.7045,0.8841)
11101	-	-	(-0.1930,0.9456)
11110	-	-	(0.8692,0.8508)
11111	-	-	(0.3263,0.9270)

[5] D. Lavery, M. Ionescu, S. Makovejs, E. Torrenco, and S. J. Savory, “A long-reach ultra-dense 10 Gbit/s WDM-PON using a digital coherent receiver,” *Opt. Express* vol. 18, no. 25, pp. 25855-25860 (2010).  
 [6] D. Lavery, C. Behrens, and S. Savory, “A comparison of modulation formats for passive optical networks,” *Opt. Express* vol. 19, no. 26, pp. B836-B841 (2011).  
 [7] E. Agrell and M. Karlsson, “Power-Efficient Modulation Formats in Coherent Transmission Systems,” *J. Lightwave Technol.*, vol. 27, no. 22, pp. 5115-5126, Nov., 2009.  
 [8] A. Alvarado, T. Fehenberger, B. Chen and F. M. J. Willems, “Achievable Information Rates for Fiber Optics: Applications and Computations,” *J. Lightwave Technol.*, vol. 36, no. 2, pp. 424-439, 15 Jan.15, 2018.  
 [9] G. Liga, A. Alvarado, E. Agrell, and P. Bayvel, “Information rates of next-generation long-haul optical fiber systems using coded modulation,” *J. Lightwave Technol.*, vol. 35, pp. 113-123, no. 1, Jan., 2017.  
 [10] L. Schmalen, A. Alvarado, and R. Rios-Müller, “Performance prediction of nonbinary forward error correction in optical transmission experiments,” *J. Lightwave Technol.*, vol. 35, pp. 1015-1027, no. 4, Feb., 2017.  
 [11] A. Alvarado and E. Agrell, “Four-dimensional coded modulation with bit-wise decoders for future optical communications,” *J. Lightwave Technol.*, vol. 33, pp. 1993-2003, no. 10, May 2015.  
 [12] A. Alvarado, E. Agrell, D. Lavery, R. Maher, and P. Bayvel, “Replacing the soft-decision FEC limit paradigm in the design of optical communication systems,” *J. Lightwave Technol.*, vol. 33, pp. 707-721, no. 20, Oct. 2015.  
 [13] M. Ionescu *et al.*, “74.38 Tb/s Transmission Over 6300 km Single Mode Fiber with Hybrid EDFA/Raman Amplifiers,” Paper Tu3F.3 in Proc. 2019 Optical Fiber Communications Conference and Exhibition (OFC), San Diego, CA, USA, 2019, pp. 1-3.  
 [14] F. Schreckenbach, N. Görtz, J. Hagenauer, G. Bauch, “Optimization of symbol mappings for bit-interleaved coded modulation with iterative decoding,” *IEEE Commun. Lett.*, vol. 7, no. 12, pp. 593-595, Dec. 2003.  
 [15] B. Chen, C. Okonkwo, D. Lavery and A. Alvarado, “Geometrically-shaped 64-point Constellations via Achievable Information Rates,” 2018

- 20th International Conference on Transparent Optical Networks (ICTON), Bucharest, 2018, pp. 1-4.
- [16] B. Chen, C. Okonkwo, H. Hafermann and A. Alvarado, "Increasing Achievable Information Rates via Geometric Shaping," in Proc. European Conference on Optical Communication (ECOC), 2018, pp. 1-3.
  - [17] L. Schmalen, A. Alvarado and R. Rios-Muller, "Predicting the performance of nonbinary forward error correction in optical transmission experiments," Paper M2A.2 in Proc. Optical Fiber Communications Conference and Exhibition (OFC), 2016, pp. 1-3.
  - [18] C. Behrens, D. Lavery, R. I. Killely, S. J. Savory, P. Bayvel, "Long-haul WDM transmission of PDM-8PSK and PDM-8QAM with nonlinear DSP," Paper OM3A.4 in Proc. Optical Fiber Communication Conference, 2012.
  - [19] R. Rios-Müller, J. Renaudier, L. Schmalen, and G. Charlet, "Joint Coding Rate and Modulation Format Optimization for 8QAM Constellations Using BICM Mutual Information," Paper W3K.4 in Proc. Optical Fiber Communication Conference, 2015.
  - [20] Cable Television Laboratories Inc. "Data-Over-Cable Service Interface Specifications DOCSIS<sup>®</sup> 3.1" CM-SP-PHYv3.1 Jan. 2019.
  - [21] K. Kikuchi and S. Tsukamoto, "Evaluation of Sensitivity of the Digital Coherent Receiver," J. Lightwave Technol., vol. 26, no. 13, pp. 1817-1822, July, 2008.
  - [22] S. Zhang *et al.*, "Flex-Rate Transmission using Hybrid Probabilistic and Geometric Shaped 32QAM," paper M1G.3 in Proc. Optical Fiber Communication Conference, 2018.
  - [23] M. Yang, L. Li, X. Liu, and I. B. Djordjevic, "FPGA-Based Real-Time Soft-Decision LDPC Performance Verification for 50G-PON," paper W3H.2 in Proc. Optical Fiber Communication Conference, 2019.
  - [24] D. Lavery *et al.*, "Opportunities for optical access network transceivers beyond OOK [invited]," IEEE/OSA Journal of Optical Communications and Networking, vol. 11, no. 2, pp. A186-A195, Feb. 2019.
  - [25] I. N. Cano, A. Lerin, V. Polo, and J. Prat, "Polarization independent single-PD coherent ONU receiver with centralized scrambling in udWDM-PONs," in Proc. Eur. Conf. Opt. Commun., 2014, Paper P.7.12.
  - [26] T. G. Hodgkinson, R. A. Harmon and D. W. Smith, "Polarisation-insensitive heterodyne detection using polarisation scrambling," in Electronics Letters, vol. 23, no. 10, pp. 513-514, May 1987.
  - [27] S. C. Davies *et al.*, "Narrow linewidth, high power, high operating temperature digital supermode distributed Bragg reflector laser," paper Th.1.B.3 in Proc. of European Conference on Optical Communication, 2013.
  - [28] A. Mecozzi, C. Antonelli and M. Shtaif, "Kramers-Kronig coherent receiver," in Optica, vol. 3, no. 11, pp. 1220-1227, Nov 2016.
  - [29] M. Mazur *et al.*, "Optimization of low-complexity pilot-based DSP for high spectral efficiency  $51 \times 24$  Gbaud PM-64QAM transmission," paper Mo4F.2. in Proc. of European Conference on Optical Communication, 2018.
  - [30] Y. Wakayama *et al.*, "Increasing Achievable Information Rates with Pilot-Based DSP in Standard Intradynne Detection" paper W.1.B.5 in Proc. of European Conference on Optical Communication, 2019.
  - [31] S. Savory, "Digital filters for coherent optical receivers," in Optics Express, vol. 16, no. 2, pp. 804-814, 2008.
  - [32] E. Agrell, "Database of sphere packings." 2016. [Online]. Available:<http://codes.se/packings>